Pinning down the strength function for ordinary muon capture on ^{100}Mo

L. Jokiniemi [a,*], J. Suhonen [a], H. Ejiri [b], I.H. Hashim [c]

[a] *University of Jyvaskyla, Department of Physics, P.O. Box 35, FI-40014, Finland*
[b] *Research Center for Nuclear Physics, Osaka University, Ibaraki, Osaka 567-0047, Japan*
[c] *Physics Department, Faculty of Science, Universiti Teknologi Malaysia, 81310 Johor Bahru, Malaysia*

A B S T R A C T

Ordinary muon capture (OMC) on ^{100}Mo is studied both experimentally and theoretically in order to access the weak responses in wide energy and momentum regions. The OMC populates states in ^{100}Nb up to some 50 MeV in excitation energy. For the first time the associated OMC strength function has been computed and compared with the obtained data. The present computations are performed using the Morita-Fujii formalism of OMC by extending the original formalism beyond the leading order. The participant nuclear wave functions are obtained in extended no-core single-particle model space using the spherical version of proton-neutron quasiparticle random-phase approximation (pnQRPA) with two-nucleon interactions based on the Bonn one-boson-exchange G matrix. Partial restoration of the isospin symmetry is implemented in the calculations by separately fitting the isoscalar and isovector parts of the particle-particle interaction strength of pnQRPA. Both the computed and experimental OMC strength distributions show a giant resonance at around 12 MeV. Further measurements and calculations of the OMC strength functions for double-beta-decay daughter nuclei could enable access to in-medium renormalization of the weak axial couplings and pave the way to improved accuracy of the double-beta-decay nuclear matrix elements.

In the ordinary muon capture (OMC) a negative muon on an atomic orbit is captured by the atomic nucleus quite like in the ordinary electron capture of a nucleus, except that the rest mass of the muon is some 200 times the rest mass of an electron. Due to the large momentum exchange, $q \sim 50$–100 MeV/c, in the process, the OMC can lead to final states that are both highly excited and of high multipolarity J^π, quite like in the analogous process of the neutrinoless double beta ($0\nu\beta\beta$) decay where the Majorana-neutrino exchange with $q \sim 100$ MeV induces high-excitation and high-multipolarity transitions through the virtual states of the intermediate nucleus. This analogue leads immediately to the idea of using the OMC as probe of the nuclear matrix elements (NMEs) involved in the $0\nu\beta\beta$ decays. This probe corresponds to the right branch (β^+ type of transitions) of the $0\nu\beta\beta$ virtual transitions.

As mentioned above, one of the incentives of the OMC studies is related to the $0\nu\beta\beta$ decays [1,2] and to neutrino-nucleus interactions in general (see the recent review [3]). General aspects of these relations have been treated also in the reviews [4–9] and the associated $0\nu\beta\beta$ NMEs have been discussed e.g. in [1,10,11]. The muon-capture processes concern β^+ type of transitions from a nucleus ^A_ZX to the states of the residual nucleus $^{A}_{Z-1}$Y (see the review [12]). Nuclear-structure calculations for the OMC transitions have been performed in a wide range of nuclear masses along the years. In these calculations the muon-capture transitions have been used to probe the right-leg (the β^+ side) virtual transitions of $0\nu\beta\beta$ decays and the value of the particle-particle interaction parameter g_{pp} of the pnQRPA, as discussed in [13–15]. The OMC calculations can also be used to yield information on the in-medium renormalization of the axial current in the form of an effective strength of the weak axial-vector coupling g_A [16–21]. For the experimental aspects of the axial-vector coupling see the reviews [3,4,22,23]. The involved large momentum exchange in the OMC activates the induced weak currents quite like in the case of the $0\nu\beta\beta$ decay [24]. These induced terms include the weak magnetism and pseudoscalar contributions, the magnitude of the induced pseudoscalar term being a very interesting unknown in finite atomic nuclei [16, 17,25–31]. A recent review on the renormalization of g_P is given in [32].

Experimentally, it has been shown that mass distributions of residual isotopes from the OMC can be used to study astro-(anti)neutrino β^+ type of strength distribution and the associated giant resonances in the high-excitation regions [3,33,34]. The OMC probe is also used to study nuclear responses for medium-energy astro-(anti)neutrinos (μ and τ (anti)neutrinos from supernovae) [3,4]. Weak $\beta^\pm$ responses and giant resonances have been discussed before in [4,22,23].

In the present work we study both theoretically and experimentally the OMC on ^{100}Mo populating states in ^{100}Nb in a wide excitation region, up to some 50 MeV. The rate of OMC to individual final states forms a strength function quite like in the case of (n,p) charge-exchange reactions for 1^+ final states (the Gamow-Teller strength function). The OMC strength function contains giant resonances analogously to the Gamow-Teller giant resonance [35] or isovector spin-monopole [36,37] and higher isovector spin-multipole resonances [3,4,22,38], and here we study the structure of these resonances. This is the first time such resonances are being studied both theoretically and experimentally, inspired by the first observation of the OMC giant resonance at around 12 MeV [3,39,40]. Eventual extension of the experiments and calculations to other nuclei, involved in $0\nu\beta\beta$ decays, helps theories better evaluate the β^+ NMEs associated with the $0\nu\beta\beta$ decays and the NMEs related to astro-(anti)neutrino interactions. In addition, the effective values of the axial-vector coupling g_A and induced pseudoscalar coupling g_P play essential roles both in $0\nu\beta\beta$ decays and OMC [41].

The OMC process we are interested in here can be written as

$$\mu^- + {}^A_Z X(0^+) \rightarrow \nu_\mu + {}^A_{Z-1} Y(J^\pi) \,, \qquad (1)$$

where the muon (μ^-) is captured by the 0^+ ground state of the even-even nucleus X of mass number A and atomic number Z leading to the J^π states of its odd-odd isobar Y of atomic number $Z - 1$; here J is the angular momentum and π the parity of the final state. At the same time a muon neutrino ν_μ is emitted. The OMC on a nucleus ${}^A_Z X$ populates excited states in a wide excitation region of the residual nucleus ${}^A_{Z-1} Y$. They de-excite by emitting γ rays to the ground state of ${}^A_{Z-1} Y$ or by emitting mostly the first neutron to a state in a nucleus ${}^{A-1}_{Z-1} Y'$, depending on whether the excitation energy is below or above the first neutron-emission threshold energy. The residual nucleus ${}^{A-1}_{Z-1} Y'$, after the first neutron emission, de-excites by emitting γ rays to the ground state of ${}^{A-1}_{Z-1} Y'$ or by emitting a second neutron, depending on whether the excitation energy is below or above the second neutron-emission threshold energy, and so on. Then, one finally ends up with the residual isotopes of ${}^{A-x}_{Z-1} Y'$ with $x = 0, 1, 2, 3,...,$ depending on the excitation energy E and the number x of the emitted neutrons. Here proton emissions are suppressed by the Coulomb barrier in medium-heavy and heavy nuclei.

The OMC on ^{100}Mo was studied at the MuSIC beam channel at RCNP and the D2 beam channel in J-PARC MLF [40,42]. The nucleus ^{100}Mo is one of DBD nuclei, and is used also for solar- and supernova-neutrino studies [6,34,43,44]. The delayed γ-ray characteristics of the residual radioactive isotopes of $^{100-x}$Nb were measured, and the number of the Nb residual isotopes $^{100-x}$Nb produced by the OMC on ^{100}Mo was evaluated from the observed γ-ray yields. The 1^+ strength can produce the Gamow-Teller component of the OMC giant resonance. The vector 1^- and axial-vector 2^- spin-dipole strengths with $1\hbar\omega$ jump show broad giant-resonance-like distributions similarly to the isovector spin-dipole (p,n)-type of charge-exchange resonance [38]. The Gamow-Teller and spin-dipole resonances have also been discussed in [22, 45]. The corresponding OMC distributions, being of (n,p) charge-exchange type [22], are shown later in this article.

A powerful formalism for the calculation of the OMC rates in muonic atoms was developed by Morita and Fujii in [46]. In the present calculations we use a similar formalism by writing the partial muon capture rate to a J^π final state as

$$W = 8 \left(\frac{Z_{\text{eff}}}{Z} \right)^4 P (\alpha Z m'_\mu)^3 \frac{2J_f + 1}{2J_i + 1} \left(1 - \frac{q}{m_\mu + AM} \right) q^2 \,, \qquad (2)$$

where A denotes the mass number of the initial and final nuclei, J_i (J_f) the angular momentum of the initial (final) nucleus, M the average nucleon rest mass, m_μ the bound muon mass (the rest mass minus the binding energy of the muon in the K orbital of the μ-mesonic atom), m'_μ the muon reduced mass in the parent μ-mesonic atom, Z atomic number of the initial nucleus, α the fine-structure constant and q the magnitude of the exchanged momentum between the captured muon and the nucleus [46], i.e. the Q value of the OMC (momentum of the emitted muon neutrino). The Q value can be obtained from

$$q = (m_\mu - W_0) \left(1 - \frac{m_\mu - W_0}{2(M_f + m_\mu)} \right) \,, \qquad (3)$$

where $W_0 = M_f - M_i + m_e + E_X$ [46]. Here M_f and M_i are the nuclear masses of the final and initial nuclei, m_e the electron rest mass and E_X is the excitation energy of the final-state nucleus. For the heavy nuclei the atomic orbit of the muon penetrates the nucleus and the capture rate has to be corrected for the muonic screening. Here we follow the Primakoff procedure [47] where the capture rate has been corrected by the factor $(Z_{\text{eff}}/Z)^4$, where the effective atomic number is obtained from the work of Ford and Wills [48], giving $Z_{\text{eff}} = 26.37$ in the present case. The term P in Eq. (2) has a complex structure, containing all the nuclear matrix elements, as well as weak couplings, Racah coefficients and some geometric factors. For the exact form see Eq. (45) in the paper of Morita and Fujii [46].

For nth forbidden OMC transitions the P term in (2) can be expanded in powers of the small quantity $1/M^2$. In this way one ends up with the explicit formula $P = P_0 + P_1$, where P_0 is the part which one obtains by neglecting all terms of order $1/M^2$ (except for terms containing g_P^2, which is large compared with the other coupling constants) and P_1 contains the rest of the $1/M^2$ terms. The P_0 part is the explicit form that can be found in [46], Eq. (58). The next-to-leading-order term P_1 in the expansion is sometimes needed for OMC transitions which are quite weak, usually for captures to high-lying states of high multipolarity J_f^π, where π is the parity of the final state. We derived this part from Eq. (46) of [46] and introduced it into our capture-rate calculations [49].

The P term contains coefficients $g_V \equiv g_V(q)$ and $g_A \equiv g_A(q)$ that are the usual weak vector and axial-vector couplings at finite momentum transfer $q > 0$. The conserved vector current (CVC) and partially conserved axial-vector current (PCAC) hypotheses dictate for a free nucleon the values $g_V(0) = 1.00$ and $g_A(0) = 1.27$ at zero momentum transfer and the dipole approximation can be used for finite momentum transfer [3]. For these couplings deviations from the CVC and PCAC values have been recorded at zero momentum transfer (the situation with the renormalization of the weak couplings has been charted in the recent reviews [23,41]). Then one refers to effective values of these couplings. For the induced pseudoscalar coupling g_P the Goldberger-Treiman PCAC relation [50] gives $g_P/g_A = 7.0$. In order to see how the values of these coupling strengths affect the OMC strength function and the total OMC rate, we vary in this work independently the values of $g_A(0)$ and $g_P(0)$ and keep the CVC value $g_V(0) = 1.00$. Such a procedure is justified by the earlier results from the OMC studies in
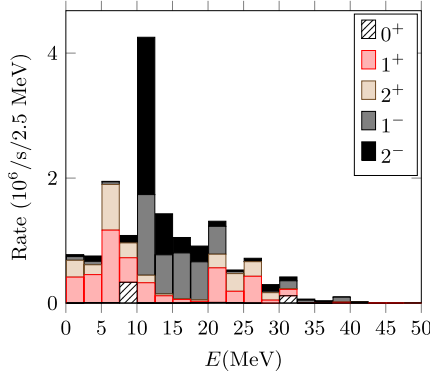
Fig. 1. Muon-capture-rate distribution (OMC strength function) including transitions to $J_f^\pi = 0^+, 1^\pm, 2^\pm$ states. The horizontal axis shows the excitation energy in the ^{100}Nb nucleus. Here a 2.5 MeV binning in energy is used in order to match the energy binning used in the experimental data analysis. Parameter values $g_A(0) = 0.8$ and $g_P(0) = 7.0$ were adopted in the calculations.

Fig. 2. The same as in Fig. 1 but with the transitions to the rest of the possible multipole final states J_f^π added.

Fig. 3. The same as in Fig. 1 but for multipole states $J_f^\pi = 3^\pm, 4^\pm$.

light, medium-heavy and heavy nuclei (see e.g. [19,20,31] and the review [32]) where renormalized values of g_A and g_P, breaking the Goldberger-Treiman PCAC relation, were recorded.

In the numerical computations we used no-core single-particle bases for both protons and neutrons. The bases contained all orbitals up to the $0i - 1g$ oscillator shell, i.e. 7 full oscillator shells (see [38]). This single-particle basis is thus able to catch $n\hbar\omega$ excitations for $n \leq 6$. The corresponding single-particle energies were obtained using the Woods-Saxon (WS) potential with the parametrization of [51], suitable for nuclei which lie close to the β-decay stability line, like ^{100}Mo. Some adjustments of the WS single-particle energies were made near the corresponding Fermi surfaces in order to improve the quality of the one-quasiparticle spectra. These details were addressed in our paper [52] and the reader is referred to it for further information.

The nuclear Hamiltonian was obtained from the Bonn-A one-boson-exchange potential introduced in [53]. The BCS pairing gaps are adjusted to the phenomenological pairing gaps by adjustable pairing strengths for protons and neutrons in a way described in [38] where isovector spin-multipole giant resonances were treated in the same formalism.

The wave functions and energies of the complete set of J_f^π multipole states are obtained by performing a pnQRPA diagonalization in the unperturbed basis of quasiproton-quasineutron pairs coupled to J_f^π (see, e.g., [1,54–56]. All the particle-hole G-matrix elements are multiplied by a factor g_{ph} the value of which is adjusted to the centroid of the Gamow-Teller giant resonance in the nucleus ^{100}Tc. The isoscalar ($T = 0$) and isovector ($T = 1$) parts of the particle-particle G-matrix elements are multiplied by factors $g_{pp}^{T=0}$ and $g_{pp}^{T=1}$ that are adjusted according to isospin-symmetry restoration scheme introduced in [57] as explained in detail in the double-β-decay paper [52].

The capture rates for the transitions $\mu^- + {}^{100}\text{Mo}(0_{gs}^+) \rightarrow \nu_\mu + {}^{100}\text{Nb}(J_f^\pi)$ were computed for all multipole states J_f^π and the data applies to multipole states $J_f^\pi = 0^+, 1^\pm, 2^\pm$. In the present calculations we have varied independently the values of the axial-vector coupling $g_A(0)$ and the induced pseudoscalar coupling $g_P(0)$ and keep the CVC value $g_V(0) = 1.00$ of the vector coupling. Furthermore, we have varied these parameters in the ranges of $g_A(0) = 0.6 - 1.27$ (this is a reasonable range as discussed in the review [41]) and $g_P(0) = 0 - 10$ in order to see how they affect the total capture rate and the structure of the OMC strength function.

In Fig. 1 we present the OMC rate distribution (OMC strength function) of transitions to the lowest multipole states $J_f^\pi =$
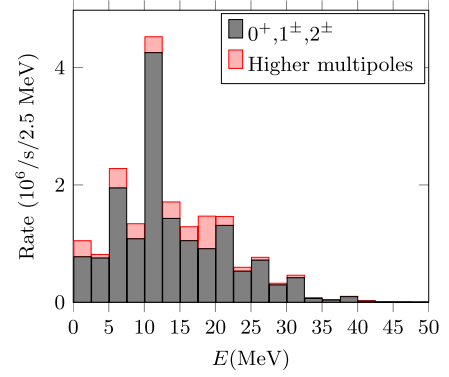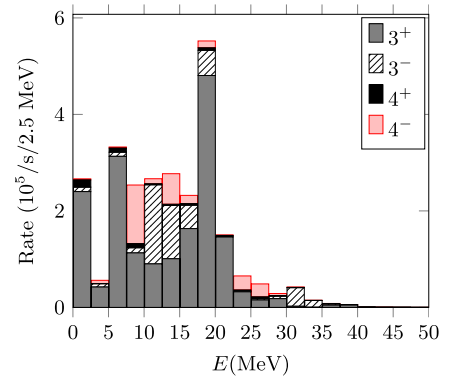
$0^+, 1^+, 2^+, 1^-$ and 2^-. We notice that transitions to $J_f^\pi = 1^-, 2^-$, which are $1\hbar\omega$ excitations, have the highest capture rates and that these multipoles are the ones that are primarily responsible of the OMC giant resonance at around 12 MeV of excitation. The OMC to multipole states 1^+ and 2^+ forms a satellite resonance at around 7 MeV. These are $0\hbar\omega$ excitations, together with the low-lying 0^+ strength. The higher-lying 0^+, 1^+ and 2^+ strength, beyond some 20 MeV, stems from $2\hbar\omega$ excitations and the 1^- and 2^- strength in this high-excitation region stems from $3\hbar\omega$ excitations. It should be noted that the (p,n)-type charge-exchange 1^+ Gamow-Teller giant resonance is quite strong and peaked but here this resonance is diluted since OMC is an (n,p) type of charge-exchange mechanism where for medium-heavy and heavy nuclei the relative locations of the proton and neutron Fermi surfaces hinder $0\hbar\omega$ excitations.

In Fig. 2 we present the total OMC rate to all multipoles. We separate the total capture rates to two parts: strength containing either the lowest-multipole ($J_f^\pi = 0^+, 1^\pm, 2^\pm$) states or the higher-multipole states. We notice that approximately $80 - 90\%$ of the total capture rate consists of transitions to the lowest multipoles, and the rest $10 - 20\%$ comes from the transitions to higher multipoles. The contributions of some of the leading higher multipoles ($J_f^\pi = 3^\pm, 4^\pm$) are presented in Fig. 3. It can be seen that the overwhelming contribution comes from the $0\hbar\omega$ and $2\hbar\omega$ 3^+ multipole, the $1\hbar\omega$ 3^- and 4^- contributions being the sub-leading ones. The 4^+ contribution is negligible.

In Table 1 we show the ratio $W_A(J_f^\pi)/W(J_f^\pi)$, where $W_A(J_f^\pi)$ contains only the axial part of the total capture rate $W(J_f^\pi)$ to the multipole states J_f^π. The OMC rate to 0^+ states is purely vector and is not displayed in the table. From the table one sees that the axial contribution increases with increasing value of $g_A(0)$ and

Table 1

Axial-vector contribution to the total capture rate ($W_A(J_f^\pi)/W(J_f^\pi)$) to final states $J_f^\pi = 1^\pm, 2^\pm$ for different values of $g_A(0)$. The values are calculated using pseudoscalar strength $g_P(0) = 7.0$.

$g_A(0)$	Final-state multipole J_f^π			
	1^+	2^+	1^-	2^-
0.6	0.65	0.22	0.26	0.66
0.8	0.72	0.32	0.36	0.74
1.0	0.77	0.40	0.45	0.79
1.27	0.82	0.49	0.54	0.83
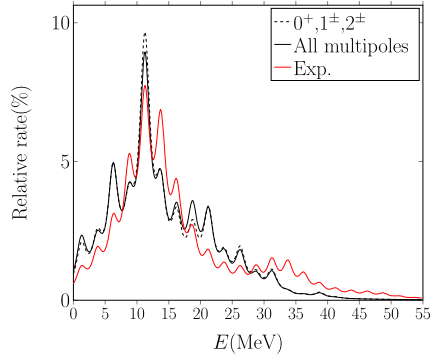
Fig. 4. Comparison of different relative (in per cents) muon-capture-rate distributions: theoretical capture rates to $J_f^\pi = 0^+, 1^\pm, 2^\pm$ states, and to all possible states, compared with the experimental strength distribution. The theoretical rates were computed with parameter values $g_A(0) = 0.8$ and $g_P(0) = 7.0$. The original energy-binned distributions are smeared by a Lorentzian folding function for clearer presentation.

that the OMC to 1^+ and 2^- states is mostly axial and very similar for both multipoles. The capture rate for the 1^- and 2^+ states is mostly vector with a similar ratio for both multipoles.

In Fig. 4 we plot the theoretical and experimental relative capture-rate distributions against each other. The distributions are smeared by a Lorentzian folding function for easier comparison of the different distributions. Here the experimental giant resonances GR1 at around 12 MeV and GR2 at around 30 MeV were derived from the OMC residual-isotope distributions using the neutron equilibrium-emission and pre-equilibrium-emission models as given in [33,40]. There are two different theoretical capture-rate distributions, one including the transitions to the lowest multipole ($J_f^\pi = 0^+, 1^\pm, 2^\pm$) states and the other containing transitions to all multipole states. We notice that the overall features of all the relative rate distributions are similar: there is a strong peak, GR1, around $10 - 12.5$ MeV and tails on both sides. However, the experimental distribution is a bit more spread to higher energies as compared to the theoretical distributions, containing also the GR2 bump. Here it should be noted that the strength at around 30 MeV, which is analyzed in terms of the second giant resonance GR2, includes some experimental and analysis uncertainties, and thus requires further studies to confirm the amount of the high-energy strength. It is interesting to note that the experimental rates are spread beyond 30 MeV, suggesting some spread of GR strengths with higher multipoles of $J^\pm$ with $J \geq 3$ and n (radial node) ≥ 2. Similar effect was observed beyond the SD GR region (30 MeV) in case of (^{3}He,t) charge exchange reactions [3]. Also, in the theoretical distributions, there is a satellite (consisting mainly of transitions to $J_f^\pi = 1^+, 2^+$ states) that is absent in the experimental distribution or shifted to higher energy. There are no notable differences between the two theoretical distributions.

In Table 2 we present the total OMC rates obtained by using different values for $g_A(0)$ and $g_P(0)$. If we compare the computed values with the total capture rate $W = 7.7 \times 10^6$ 1/s evaluated

Table 2

Total rates of muon capture by ^{100}Mo for different values of the pseudoscalar and axial-vector strengths $g_P(0)$ and $g_A(0)$. The rates are expressed in units of $10^6/s$.

$g_A(0)$	$g_P(0) = 0$		$g_P(0) = 7$		$g_P(0) = 10$	
	$W_{(0^+,1^\pm,2^\pm)}$	W_{tot}	$W_{(0^+,1^\pm,2^\pm)}$	W_{tot}	$W_{(0^+,1^\pm,2^\pm)}$	W_{tot}
0.6	11.8	13.8	10.8	12.4	10.7	12.2
0.8	17.0	20.2	15.7	18.3	15.3	17.7
1.0	23.9	28.4	28.0	31.9	21.2	24.8
1.27	34.8	41.7	32.2	38.2	31.3	37.0
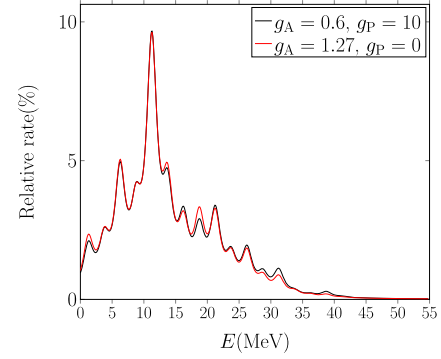
Fig. 5. The relative OMC-rate distributions using two different parameter sets: $g_A(0) = 0.6$ and $g_P(0) = 10$, and $g_A(0) = 1.27$ and $g_P(0) = 0$. The distributions are smeared by a Lorentzian folding function.

by using the Primakoff approximation (see Eq. (4.53) of the review article [12]), we notice that the Primakoff value is smaller than the theoretical rates. Increasing the value of $g_P(0)$ or decreasing the value of $g_A(0)$ decreases the theoretical total capture rate, and the closest value to the Primakoff value is achieved by using $g_A(0) = 0.6$ and $g_P(0) = 10$, leading to $g_P(0)/g_A(0) = 16.7$, much larger than the PCAC value of 7.0. It is evident from the table that the total rate is quite insensitive to the value of $g_P(0)$ and not too much can be said about the value of $g_P(0)$ based on the total OMC rates. The differences between the computed and Primakoff total OMC rates are partly related to the higher average energy (smaller phase space) of the experimental OMC strength function and partly to the possible quenching of the effective weak couplings $g_A(0)$ and $g_P(0)$. Comparison of the computed and Primakoff total capture rates suggests a strongly quenched effective value of $g_A(0) \approx 0.5$, which is in accord with the results of many earlier β-decay studies (see e.g. [58–62]). From Table 2 one can also see that a decrease of $g_A(0)$ by a factor of 2 results in reduction of the rate by a factor of 3, not by a factor of 4, due to the vector components, as in the case of $0\nu\beta\beta$ NMEs [3,23,63]. It should also be noted that the considered variation in the values of $g_A(0)$ and $g_P(0)$ does not affect noticeably the shape of the computed capture-rate distribution as visible in Fig. 5 where we plot the Lorentzian folding of the total rate distributions computed for parameter-value pairs of $g_A = 0.6$ and $g_P = 10$, and $g_A = 1.27$ and $g_P = 0$.

In this Letter we show for the first time a direct comparison between the experimental and computed distributions of muon-capture rates to low-multipole J_f^π states in a daughter nucleus. The presently discussed case is the ordinary muon capture (OMC) on the 0^+ ground state of ^{100}Mo leading to $J_f^\pi = 0^+, 1^\pm, 2^\pm$ states in ^{100}Nb. The experimental distribution and the OMC giant resonance are based on the recent measurement of the γ rays in the residual ions produced by the OMC. The computations were performed using the Morita-Fujii formalism of the OMC and treating the involved nuclear matrix elements by using the proton-neutron quasiparticle random-phase approximation with two-nucleon in-

teractions based on the Bonn one-boson-exchange G matrix. The nuclear Hamiltonian was taken from our earlier calculations of the locations of the isovector spin-multipole giant resonances in nuclei involved in double beta decays. Partial restoration of the isospin symmetry was achieved by the method used earlier in the context of double-beta-decay calculations.

The computed OMC strength predicts a giant resonance at around 12 MeV and thus is consistent with the recent experimental observation of the OMC giant resonance GR1 for ^{100}Mo. Calculated decomposition of the OMC strength function in terms of the involved multipoles is shown and the low-multipole strength function is compared with the one containing all multipoles. Integral over the computed complete strength function yields the total OMC rate which can be compared with the Primakoff approximation. Since the axial-vector component dominates the OMC rate, the rate is quite sensitive to the value of the weak axial coupling g_A and thus OMC can be used to study the effective value of weak axial coupling. On the other hand, the rate does not depend much on the value of the pseudoscalar coupling g_P. In our calculations we assumed the CVC value $g_V(0) = 1.00$ for the vector coupling at zero-momentum transfer. Comparison of the computed and Primakoff capture rates suggests a strongly quenched effective value of $g_A(0)$ in keeping with the results of many earlier β-decay studies. The shape of the OMC strength function is practically independent of the values of the weak axial couplings.

Further measurements and computations of the OMC strength functions for final nuclei of double beta decays would enable a systematic scan of the sensitivity of the OMC strength function to the effective in-medium values of the weak axial couplings. This, in turn, could help in improving the accuracy of calculations of the nuclear matrix elements of the neutrinoless double beta decay. Furthermore, the OMC with its large excitation energy and momentum transfer provides a unique opportunity for studying the (anti)neutrino responses for medium-energy astro-neutrino interactions. Further experimental studies are in progress at RCNP Osaka for nuclei of interest in studies of nuclear double beta decay and asto-neutrino interactions.

Acknowledgements

References

[1] J. Suhonen, O. Civitarese, Phys. Rep. 300 (1998) 123.
[2] D. Zinatulina, V. Brudanin, V. Egorov, C. Petitjean, M. Shirchenko, J. Suhonen, I. Yutlandov, Phys. Rev. C 99 (2019) 024327.
[3] H. Ejiri, J. Suhonen, K. Zuber, Phys. Rep. 797 (2019) 1.
[4] H. Ejiri, Phys. Rep. 338 (2000) 265.
[5] H. Ejiri, Prog. Part. Nucl. Sci. 54 (2010) 249.
[6] J. Vergados, H. Ejiri, F. Šimkovic, Rep. Prog. Phys. 75 (2012) 106301.
[7] J. Maalampi, J. Suhonen, Adv. High Energy Phys. 2013 (2013) 505874.
[8] J. Vergados, H. Ejiri, F. Šimkovic, Int. J. Mod. Phys. E 25 (2016) 1630007.
[9] J. Engel, J. Menendez, Rep. Prog. Phys. 60 (2017) 046301.
[10] J. Suhonen, O. Civitarese, J. Phys. G, Nucl. Part. Phys. 39 (2012) 085105.
[11] J. Suhonen, O. Civitarese, J. Phys. G, Nucl. Part. Phys. 39 (2012) 124005.
[12] D.F. Measday, Phys. Rep. 354 (2001) 243.
[13] M. Kortelainen, J. Suhonen, Europhys. Lett. 58 (2002) 666.
[14] M. Kortelainen, J. Suhonen, Nucl. Phys. A 713 (2003) 501.
[15] M. Kortelainen, J. Suhonen, J. Phys. G, Nucl. Part. Phys. 30 (2004) 2003.
[16] E. Kolbe, K. Langanke, P. Vogel, Phys. Rev. C 50 (1994) 2576.
[17] B.L. Johnson, et al., Phys. Rev. C 54 (1996) 2714.
[18] T.P. Gorringe, et al., Phys. Rev. C 60 (1999) 055501.
[19] T. Siiskonen, J. Suhonen, M. Hjorth-Jensen, J. Phys. G, Nucl. Part. Phys. 25 (1999) L55.
[20] T. Siiskonen, M. Hjorth-Jensen, J. Suhonen, Phys. Rev. C 63 (2001) 055501.
[21] N. Auerbach, B.A. Brown, Phys. Rev. C 65 (2002) 024322.
[22] H. Ejiri, Phys. Rep. 38C (1978) 85.
[23] H. Ejiri, Front. Phys. 7 (2019) 30.
[24] F. Šimkovic, G. Pantis, J.D. Vergados, A. Faessler, Phys. Rev. C 60 (1999) 055502.
[25] T.P. Gorringe, et al., Phys. Rev. Lett. 72 (1994) 3472.
[26] G. Jonkmans, et al., Phys. Rev. Lett. 77 (1996) 4512.
[27] D. Gazit, Phys. Lett. B 666 (2008) 472.
[28] L.E. Marcucci, A. Kievsky, S. Rosati, R. Schiavilla, M. Viviani, Phys. Rev. Lett. 108 (2012) 052502.
[29] V. Brudanin, et al., Nucl. Phys. A 587 (1995) 577.
[30] T. Siiskonen, J. Suhonen, V.A. Kuz'min, T.V. Tetereva, Nucl. Phys. A 635 (1998) 446; Erratum: Nucl. Phys. A 651 (1999) 437.
[31] T. Siiskonen, J. Suhonen, M. Hjorth-Jensen, Phys. Rev. C 59 (1999) R1839.
[32] T. Gorringe, H.W. Fearing, Rev. Mod. Phys. 76 (2004) 31.
[33] H. Ejiri, Proc. Int. Conf. Nuclear Structures Studied Using Electron Scattering and Photo Nuclear Reaction, Research Rep. Lab. Nucl. Sci., vol. 5, Tohoku Univ., 1972, p. 261.
[34] H. Ejiri, J. Phys. Soc. Jpn. 74 (2005) 2101.
[35] J. Suhonen, From Nucleons to Nucleus: Concepts of Microscopic Nuclear Theory, Springer, Berlin, 2007.
[36] D.R. Bes, O. Civitarese, J. Suhonen, Phys. Rev. C 86 (2012) 024314.
[37] O. Civitarese, J. Suhonen, Phys. Rev. C 89 (2014) 044319.
[38] L. Jokiniemi, J. Suhonen, Phys. Rev. C 96 (2017) 034308.
[39] H. Ejiri, Proc. CNNP17, J. Phys. Conf. Ser. 1056 (2018) 012019.
[40] I.H. Hashim, H. Ejiri, T. Shima, K. Takahisa, Y. Kuno, A. Sato, K. Ninomiya, N. Kawamura, Y. Miyake, Phys. Rev. C 97 (2018) 014617.
[41] J. Suhonen, Front. Phys. 5 (2017) 55.
[42] H. Ejiri, et al., J. Phys. Soc. Jpn. 82 (2013) 044202.
[43] H. Ejiri, J. Engel, R. Hazama, P. Krasyev, N. Kudomi, R.G.H. Robertson, Phys. Rev. Lett. 85 (2000) 2917.
[44] H. Ejiri, J. Engel, N. Kudomi, Phys. Lett. B 530 (2002) 27.
[45] H. Ejiri, J.I. Fujita, K. Ikeda, Phys. Rev. 176 (1968) 1277.
[46] M. Morita, A. Fujii, Phys. Rev. 118 (1960) 606.
[47] H. Primakoff, Rev. Mod. Phys. 31 (1959) 802.
[48] K.W. Ford, J.G. Wills, Nucl. Phys. 35 (1968) 295.
[49] L. Jokiniemi, J. Suhonen, Phys. Rev. C (2019), submitted for publication.
[50] M.L. Goldberger, S.B. Treiman, Phys. Rev. 111 (1958) 354.
[51] A. Bohr, B.R. Mottelson, Nuclear Structure, vol. I, Benjamin, New York, 1969.
[52] L. Jokiniemi, H. Ejiri, D. Frekers, J. Suhonen, Phys. Rev. C 98 (2018) 024608.
[53] K. Holinde, Phys. Rep. 68 (1981) 121.
[54] J. Suhonen, A. Faessler, T. Taigel, T. Tomoda, Phys. Lett. B 202 (1988) 174.
[55] J. Suhonen, T. Taigel, A. Faessler, Nucl. Phys. A 486 (1988) 91.
[56] J. Suhonen, Nucl. Phys. A 700 (2002) 649.
[57] F. Šimkovic, V. Rodin, A. Faessler, P. Vogel, Phys. Rev. C 87 (2013) 045501.
[58] H. Ejiri, N. Soukouti, J. Suhonen, Phys. Lett. B 729 (2014) 27.
[59] H. Ejiri, J. Suhonen, J. Phys. G, Nucl. Part. Phys. 42 (2015) 055201.
[60] P. Pirinen, J. Suhonen, Phys. Rev. C 91 (2015) 054309.
[61] F.F. Deppisch, J. Suhonen, Phys. Rev. C 94 (2016) 055501.
[62] J. Suhonen, J. Kostensalo, Front. Phys. 7 (2019) 29.
[63] J. Suhonen, Phys. Rev. C 96 (2017) 055501.